Chapter 4

Haze Removal: Multi-Scale Edge-Weighting Based-Gradient Guided Filter

4.1 Background

Multi-scale edge weighting gradient guided filters are a image processing technique that combines edge detection, contrast enhancement, and filtering to improve the quality of the restored image. They proposed by incorporating of an edge-weighting component to the existing filter, which adjusts the output of the edge-aware filter in order to emphasize the local details better. As a result, it can improve the detail of structures and edges. Furthermore, this adaptation removes the halos, over-smoothing and color artifacts strongly. Edge-preserving gradient guided filter is a type of image processing filter which remove haze from input image more accurately and efficiently than the existing GIF [49], and WGIF [50] methods. This filter has

been shown to be effective while removing haze from image without blurring the edges. It is a local optimization based effective edge-preserving filter. This filter separate the edges of an image from fine details more efficiently than GIF [49], and WGIF [50]. The proposed filter is local linear optimization based efficient edge-preserving filter. It remove halos and over-smoothing strongly.

In this Chapter, we present a new robust scale-aware weighting-based effective edge-preserving gradient domain guided image filter (RSAW-EEPGDGIF) for single image dehazing. The important parameters related to haze removal are discussed in details.

4.1.1 Major Contributions of the Work

The major contributions of the proposed algorithm are as follows:

- A new robust scale-aware weighting based effective edge-preserving gradient domain guided image filter (RSAW-EEPGDGIF) is proposed for single image dehazing.
- The proposed filter refines the transmission map by decomposing it into effective weighted-base layer (EWBL) and effective weighted detail layer (EWDL), respectively.
- A sigmoid function-based non-linear mapping function (NLM) is employed to suppress the various artifacts and noises to enhance the gradient information in EWDL.

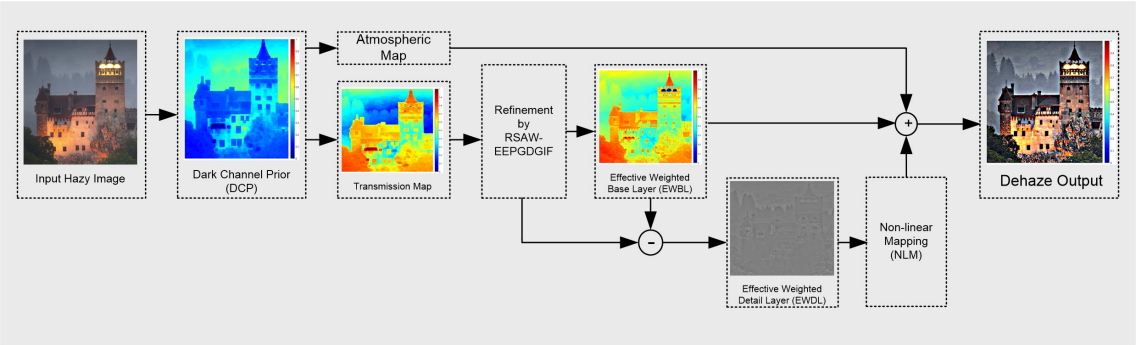

FIGURE 4.1: The basic block diagram of the proposed method.

4.2 The Proposed Algorithm

The basic block diagram of the proposed algorithm is shown in Figure 4.1. It has four steps as follows:

- In the first step, we estimate the atmospheric- and transmission- maps by dark channel prior (DCP) [15] method. DCP method estimate the atmospheric map and transmission map more accurately.
- In the next step, the initial transmission map is refined with a robust scale-aware weighting-based effective edge-preserving gradient-domain guided image filter (RSAW-EEPGDGIF). It is a multi-scale filter that refines the initial transmission map by decomposing the given image into an effective weighted-base layer (EWBL) and an effective weighted detail layer (EWDL).
- In the third step, a sigmoid function-based non-linear mapping function (NLM) is employed to suppress the various artifacts and noises to enhance the gradient information in EWDL.
- Finally, the output haze-free image is recovered from the scene radiance.

The basic flow chart of the proposed method is shown in Figure 4.2.

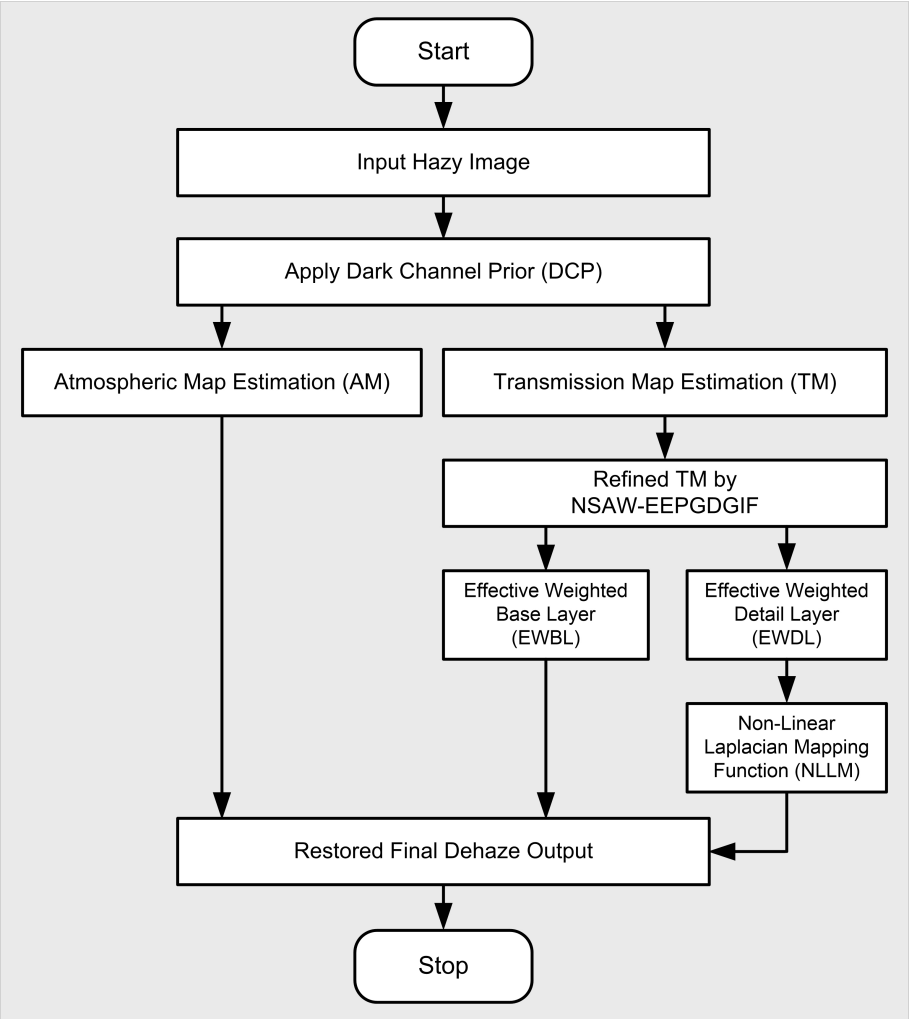

FIGURE 4.2: Flow chart of the proposed method.

4.2.1 Dark Channel Prior (DCP)-Based Transmission Map Estimation

The dark channel prior (DCP) [15] method is simple and effective approach for estimation of the atmospheric map and transmission map. In DCP [15], dark pixels concept is used to evaluate atmospheric map and transmission map accurately than the other existing methods. Among these dark pixels, the top 0.1% of brightest pixels are selected for the estimation of atmospheric map as DCP [15]. In the proposed method, dark channel prior (DCP) [15] method is used to estimate the atmospheric

map A and initial transmission map $\tilde{t}(x)$. We have already discussed the estimation of the atmospheric map A and initial transmission map $\tilde{t}(x)$ (refer to (3.24)) using DCP in Chapter 3.

4.2.2 The Proposed Filter

In this work, a new robust scale-aware weighting based effective edge-preserving gradient domain guided image filter (RSAW-EEPGDGIF) is proposed. In this filter, a new robust scale-aware weighting (RSAW) is incorporated into the cost function of the gradient guided image filter (GGIF). This filter refines the initial transmission map $\tilde{t}(x)$ accurately and removes halos and over-smoothing effects more strongly than the existing edge-preserving filters.

The proposed scale-aware weighting $\overline{\Psi}_I(k)$ is defined by local variances of I in the 3×3 and $(2\zeta_1 + 1) \times (2\zeta_1 + 1)$ for window $\omega_1(k)$ and $\omega_{\zeta_1}(k)$ as follows:

$$\overline{\Psi}_I(k) = \frac{1}{N} \sum_{i=1}^{N} \frac{T(k) + \lambda}{T(i) + \lambda}. \tag{4.1}$$

where $T(k)$ is expressed as:

$$T(k) = \frac{\sigma^2_{I,1}(k)\sigma^2_{I,\zeta_1}(k)}{\overline{\sigma}^2(k)}, \tag{4.2}$$

where $\sigma^2_{I,1}(k)$ and $\sigma^2_{I,\zeta_1}(k)$ are the variances of I in the 3×3 and $(2\zeta_1 + 1) \times (2\zeta_1 + 1)$ in a window $\omega_1(k)$ and $\omega_{\zeta_1}(k)$, respectively. $\overline{\sigma}^2(k)$ represents the average of local variances for all pixels. It can be expressed as:

$$\overline{\sigma}^2(k) = \frac{1}{N} \sum_{k=1}^{N} \sigma^2_I(k), \tag{4.3}$$

where $\sigma_I^2(k)$ is a local variance of I in window $\omega(k)$.

The novel RSAW is incorporated into the cost-function of gradient domain guided image filter (GGIF) to refine the transmission map accurately. It refines the transmission map by decomposing the input image into effective weighted-base layer (EWBL) and effective weighted detail layer (EWDL). The proposed filter removes halo artifacts and over-smoothing strongly and preserves edge informations precisely in flat and sharp regions. The cost function in the proposed filter is minimized by linear ridge regression model [63, 64]. The values of linear coefficients a_k and b_k are evaluated by minimizing the cost function $E(a_k, b_k)$ in the window $\omega_{\zeta_1}(k)$ as:

$$E(a_k, b_k) = \sum_{i(x,y)\in\omega_{\zeta_1}(k)} [(a_k I_i + b_k - p_i)^2 + \frac{\varepsilon}{\overline{\Psi}_I(k)}(a_k - \gamma_k)^2]. \tag{4.4}$$

where γ_k is defined as:

$$\gamma_k = 1 - \frac{1}{1 + e^{\eta(T(k) - \mu_{T,\infty})}}, \tag{4.5}$$

where $\mu_{T,\infty}$ represents the mean value of all $T(k)$. Next, η can be expressed as follows:

$$\eta = \frac{4}{\mu_{T,\infty} - min(T(i))}. \tag{4.6}$$

The improved optimization constant a_k is calculated by the following expression:

$$a_k = \frac{\mu_{I\odot p,\zeta_1}(k) - \mu_{I,\zeta_1}(k)\mu_{p,\zeta_1}(k) + \frac{\varepsilon}{\overline{\Psi}_I(k)}\gamma_k}{\sigma^2_{I,\zeta_1}(k) + \frac{\varepsilon}{\overline{\Psi}_I(k)}}, \tag{4.7}$$

and

$$b_k = \mu_{p,\zeta_1}(k) - a_k\mu_{I,\zeta_1}(k), \tag{4.8}$$

where $\mu_{I\odot p,\zeta_1}(k)$ represents the mean of $(I \odot p)$. For better analysis I and p can be assumed identical and it can be expressed as follows:

$$\mu_{I\odot p,\zeta_1}(k) - \mu_{I,\zeta_1}(k)\mu_{p,\zeta_1}(k) = \sigma^2_{I,\zeta_1}(k) \tag{4.9}$$

and

$$\mu_{p,\zeta_1}(k) = \mu_{I,\zeta_1}(k). \tag{4.10}$$

After substituting (4.9) and (4.10) in (4.7), we obtain

$$a_k = \frac{\sigma^2_{I,\zeta_1}(k) + \frac{\varepsilon}{\overline{\Psi}_I(k)}\gamma_k}{\sigma^2_{I,\zeta_1}(k) + \frac{\varepsilon}{\overline{\Psi}_I(k)}}, \tag{4.11}$$

and

$$b_k = (1 - a_k)\mu_{I,\zeta_1}(k), \tag{4.12}$$

or it can be simply written as:

$$a_k = \frac{\sigma^2_{I,\zeta_1}(k)}{\sigma^2_{I,\zeta_1}(k) + \frac{\varepsilon}{\overline{\Psi}_I(k)}} + \frac{\frac{\varepsilon}{\overline{\Psi}_I(k)}\gamma_k}{\sigma^2_{I,\zeta_1}(k) + \frac{\varepsilon}{\overline{\Psi}_I(k)}}. \tag{4.13}$$

As mentioned in [51], if $\gamma_k = 1$; to preserve edge information in sharp region a_k should be 1; whereas $\gamma_k = 0$; to preserve edge information in flat region a_k should be close to 0 and $\overline{\Psi}_I(k)$ is usually smaller than 1.

If we substitute these two conditions in (4.13), we obtain $a_k = 1$ for $\gamma_k = 1$ (sharp regions) and it is close to 0 for smaller $\overline{\Psi}_I(k)$ with $\gamma_k = 0$ (smooth region), as expected.

$$a_k = \frac{\sigma^2_{I,\zeta_1}(k)}{\sigma^2_{I,\zeta_1}(k) + \frac{\varepsilon}{\overline{\Psi}_I(k)}} + \frac{\frac{\varepsilon}{\overline{\Psi}_I(k)}}{\sigma^2_{I,\zeta_1}(k) + \frac{\varepsilon}{\overline{\Psi}_I(k)}} = 1, \tag{4.14}$$

$$a_k = \frac{\sigma^2_{I,\zeta_1}(k)}{\sigma^2_{I,\zeta_1}(k) + \frac{\varepsilon}{\overline{\Psi}_I(k)}} \approx 0. \tag{4.15}$$

This proves that the proposed method provides better edge preservation in both flat and sharp regions unlike the existing filters [49], [50], [51], [52], [53], [54]. After obtaining linear constants a_k and b_k, the filtered output q_i or refined transmission map $\bar{t}(x)$ can be calculated by the following expression:

$$q_i = \bar{t}(x) = (\overline{a}_i I_i + \overline{b}_i), \tag{4.16}$$

where $\overline{a}_i$ and $\overline{b}_i$ terms in the above (4.16) represent mean of a_k and b_k, respectively and can be expressed as:

$$\overline{a}_i = \frac{1}{|\omega_{\zeta_1}(i)|} \sum_{k \in \omega_{\zeta_1}(i)} a_k, \tag{4.17}$$

$$\overline{b}_i = \frac{1}{|\omega_{\zeta_1}(i)|} \sum_{k \in \omega_{\zeta_1}(i)} b_k. \tag{4.18}$$

4.2.3 Non-Linear Mapping Function (NLM)

In this section, a sigmoid function-based Laplacian decomposition method is used to enhance the gradient information in EWDL. It is a non-linear Laplacian mapping function [93, 94], which is applied on each detail layer to enhance the gradient information and suppress the artifacts. It is expressed as:

$$N(t) = \begin{cases} \frac{W}{1+\varepsilon^{-s(r-r_s)}} + r_s - W, & \text{if } -0.5W \leq r \leq 0.5W \\ t, & \text{otherwise} \end{cases} \tag{4.19}$$

where W represents width parameter and $W = 0.8$ is chosen in this work, s represents the scale factor and it is calculated by the expression $s = 50(r_{max} - r_{min})$, $r_{max} = max(R)$, $r_{min} = min(R)$ for residual (i.e. detail) term R. The shift parameter r_s is calculated as $r_s = \text{mean}(R)$.

4.2.4 Scene Recovery

Finally, the dehazed image J is calculated using the following expression:

$$J^c(x) = \frac{I^c(x) - A^c}{max(\bar{t}(x), t_0)} + A^c. \qquad c \in (r, g, b) \tag{4.20}$$

where $\bar{t}(x)$ is refined transmission map and the value of t_0 is set to 0.1 as in [49] to avoid noise amplification.

Algorithm 1 RSAW-EEPGDGIF for Single Image Dehazing

Input: Input hazy image I.

Procedure:

1: Apply dark channel prior (DCP) [15] on input hazy image and calculate atmospheric map A and transmission map $\tilde{t}(x)$

2: A new robust scale-aware weighting (RSAW) $\overline{\Psi}_I(k)$ is proposed using local variances of I in the 3×3 and $(2\zeta_1 + 1) \times (2\zeta_1 + 1)$ for window $\omega_1(k)$ and $\omega_{\zeta_1}(k)$, respectively

3: Next, $\overline{\Psi}_I(k)$ is incorporating into the cost function of guided image filter (GIF) [49] to design RSAW-based effective edge-preserving gradient domain guided image filter (RSAW-EEPGDGIF).

4: Compute the linear coefficients a_k and b_k, respectively.

5: Compute the weighted average linear coefficients $\overline{a}_k$ and $\overline{b}_k$, respectively.

6: Calculate filter output $q_i = \bar{t}(x) = (\overline{a}_i I_i + \overline{b}_i)$

7: Refine $\tilde{t}(x)$ by decomposing hazy image into effective weighted base layer (EWBL) and effective weighted detail layer (EWDL)

8: Use a sigmoid function based non-linear mapping module (NLM) [93, 94] to enhance the gradient information and suppress various artifacts

Output: Finally, restore the dehazed image $J(x)$ $J^c(x) = \frac{I^c(x) - A^c}{max(\bar{t}(x), t_0)} + A^c. \qquad c \in (r, g, b).$

4.3 Experimental Results and Discussion

The proposed method is experimented and evaluated using Matlab R2018a on a PC with Intel (R) Core (TM) i7-6700 CPU @ 3.40 GHz of a 64-bit operating system

with RAM-8GB. The performance of the proposed method is tested on hazy, non-hazy and synthetic images from different datasets viz. Fattal (120 images) [16], D-HAZY (195 images) [65], Middlebury (80 images) [68], Haze-RD (260 images) [69], Image-Net (140 images) [77], NYU2 (450 images) [66], FRIDA (400 images) [67] and O-HAZE (45 images) [71] and their outcomes are compared with different existing [15], [49], [50], [51], [52], [53], [54], [33], [35], [38], [39], [41], and [42] haze removal methods for better assessment.

4.3.1 Qualitative Analysis

In this section, we present the visual quality parameters such as; color, contrast and visibility of the proposed method and compared the results with the existing [15], [49], [50], [51], [52], [53], [54], [33], [35], [38], [39], [41], [42] haze removal methods. Results of the existing filters [49], [50], [51], [52], [53], [54] and the proposed method for four different values of ζ_1 = (5, 15, 30, 60) and fixed regularization parameter $\varepsilon = 0.1^2$ are obtained for a input image [16] and the outcomes are shown in Figure 4.3. It is clear from these figures that the halo artifacts are more visible for lower values of ζ_1, whereas it reduces as the value of ζ_1 is increases. In the case of small value of ζ_1, halo artifacts are more concentrated near the sharp regions, whereas it starts to distribute globally with the increasing values. Therefore, the visibility of halo artifacts decreases for higher values of ζ_1. It is clear from these figures that halos in sharp regions are more visible for a small ζ_1 value as compared to the large ζ_1 value. Moreover, the proposed method removes halo artifacts strongly than the existing [49], [50], [51], [52], [53], [54] methods.

Generally, the edge-preserving filters refine the initial transmission map by decomposing the haze image into a piecewise smooth, effective weighted base layer (EWBL)

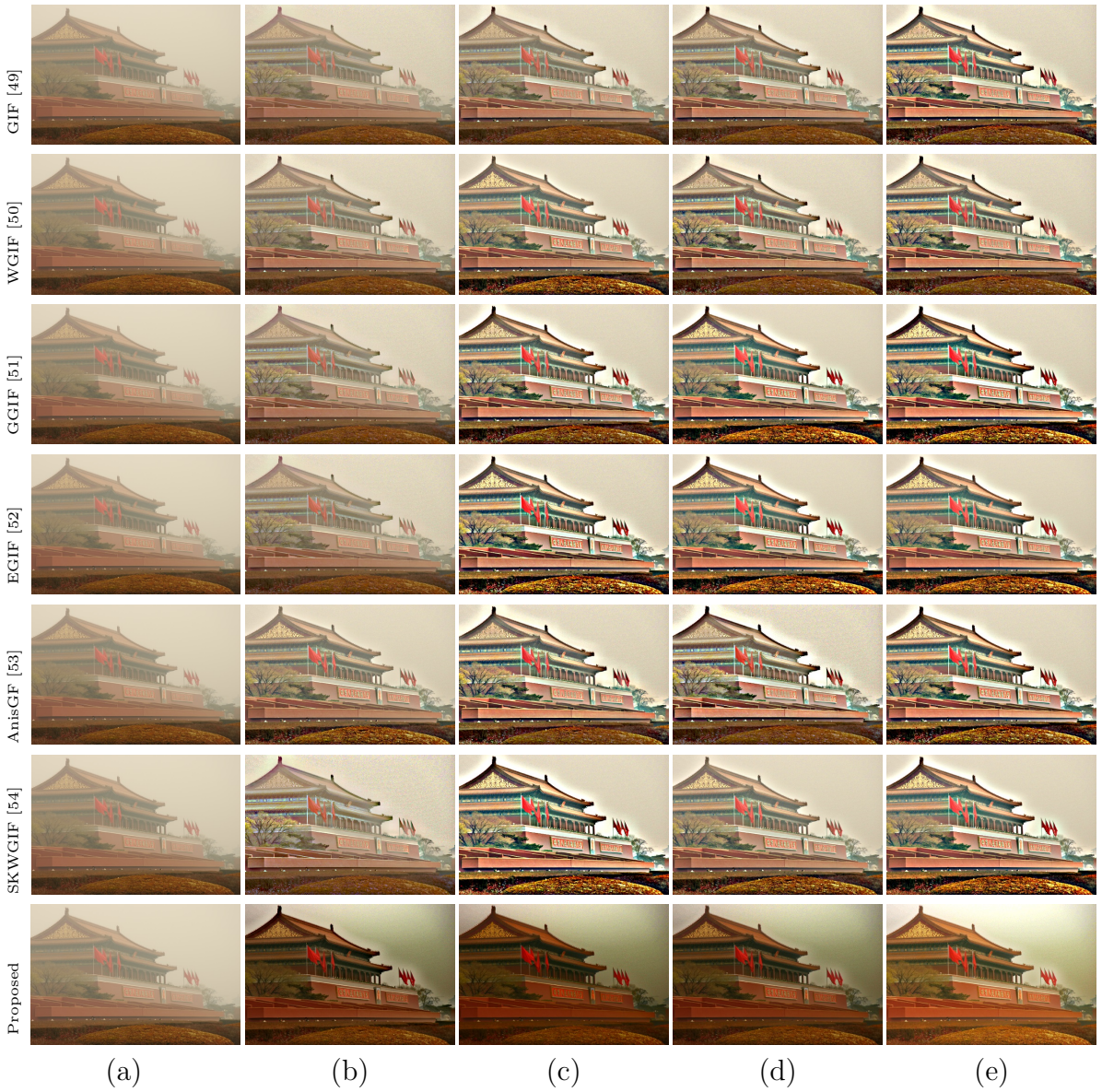

FIGURE 4.3: Dehazed outcomes of different haze removal methods. (a) Input hazy image, (b) $\zeta_1 = 5$, (c) $\zeta_1 = 15$, (d) $\zeta_1 = 30$, (e) $\zeta_1 = 60$.

with large-scale variations in the intensity domain and small-scale variations such as noise or textures in the effective weighted detail layer (EWDL). The EWBL and EWDL obtained with the proposed method and the existing [49], [50], [51], [52], [53], [54] methods for four different values of $\varepsilon = (0.001^2, 0.01^2, 0.1^2, 1^2)$ and fixed $\zeta_1 = 15$ for input tulip image [50] and their outcomes are shown in Figure 4.4 and Figure 4.5, respectively.

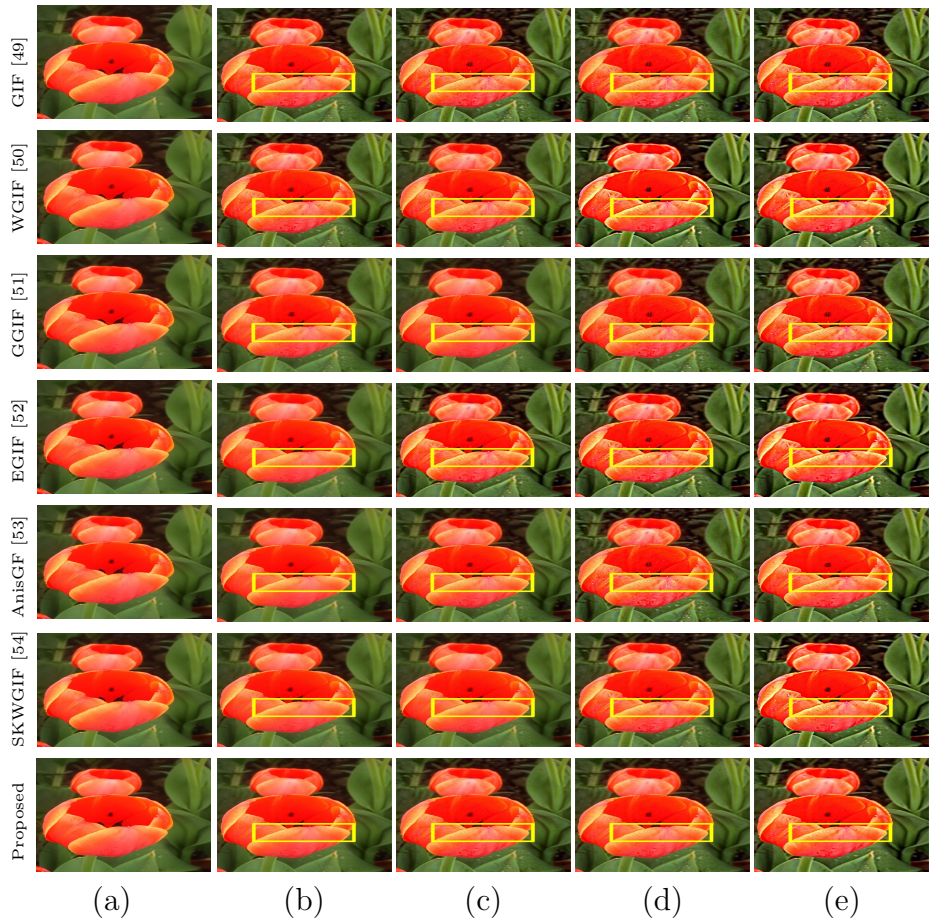

FIGURE 4.4: Effective weighted base layer (EWBL) by different edge-preserving filters. For all figures, window size $\zeta_1 = 15$ is fixed and regularization parameter ε varies. (a) Input tulip image, (b) $\varepsilon = 0.001^2$, (c) $\varepsilon = 0.01^2$, (d) $\varepsilon = 0.1^2$, (e) $\varepsilon = 1^2$.

The parameter ε is used to control the over-smoothing effects in flat and sharp regions. It is clear from these figures that the visibility of details (noises) in the existing filters and the proposed method has increased with increase in ε value. But, more detailed layers increase smoothness (over-smoothing) in the sharp regions. It is evident from Figure 4.5 that more detail layers (noise or texture) persist in the existing [49], [50], [51], [52], [53], [54] methods than the proposed method for large ε value (1^2). The EWDL in the proposed method is rarely visible in comparison to the EWDL of the existing filters [49], [50], [51], [52], [53], [54] for the same value of

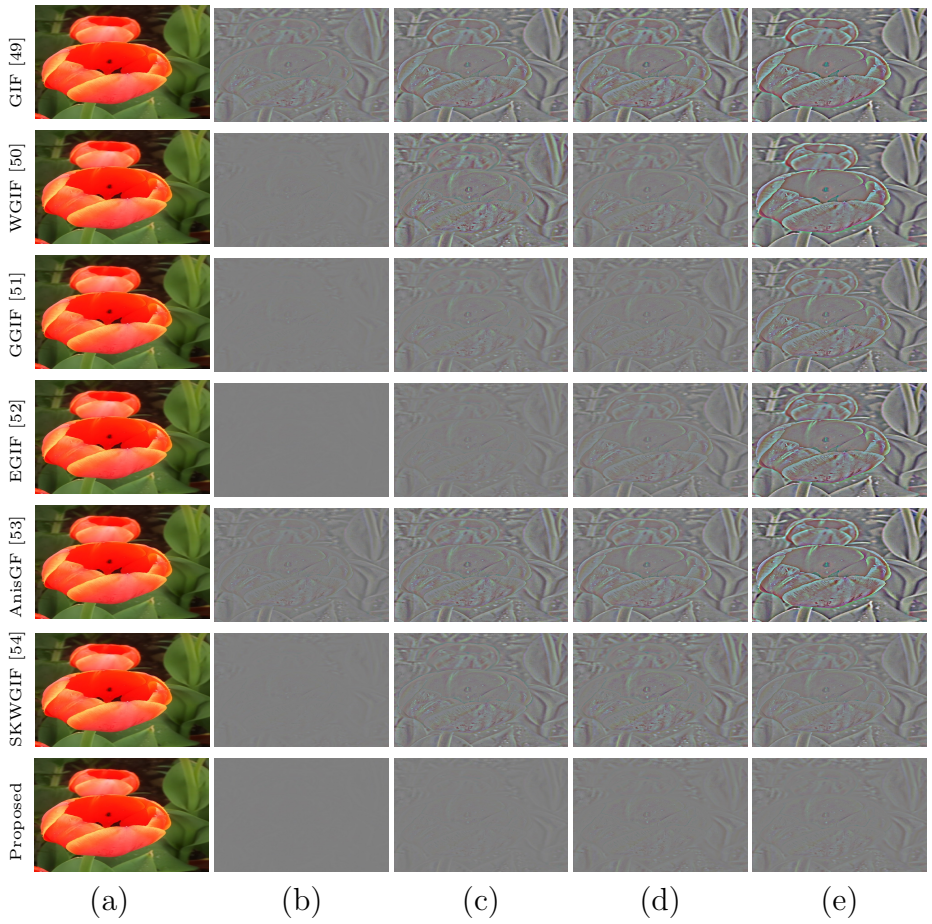

FIGURE 4.5: Effective weighted detail layer (EWDL) by different edge-preserving filters. For all figures, window size $\zeta_1 = 15$ is fixed and regularization parameter ε varies. (a) Input tulip image, (b) $\varepsilon = 0.001^2$, (c) $\varepsilon = 0.01^2$, (d) $\varepsilon = 0.1^2$, (e) $\varepsilon = 1^2$.

ε. This proves that the proposed method removes halo artifacts and over-smoothing strongly in both flat and sharp regions than the existing [49], [50], [51], [52], [53], [54] methods. The refined transmission map of the proposed method and the existing [49], [50], [51], [52], [53], [54] methods are calculated and shown in Figure 4.6. It is clear from the results shown in Figure 4.6 that the proposed method refines the transmission map more accurately than the existing haze removal methods. The DCP method presents color distortion for large sky region. Moreover, it is not applicable for large sky regions. The GIF and other existing filters are local linear-based image smoothing filters while the proposed method is a multi-scale based

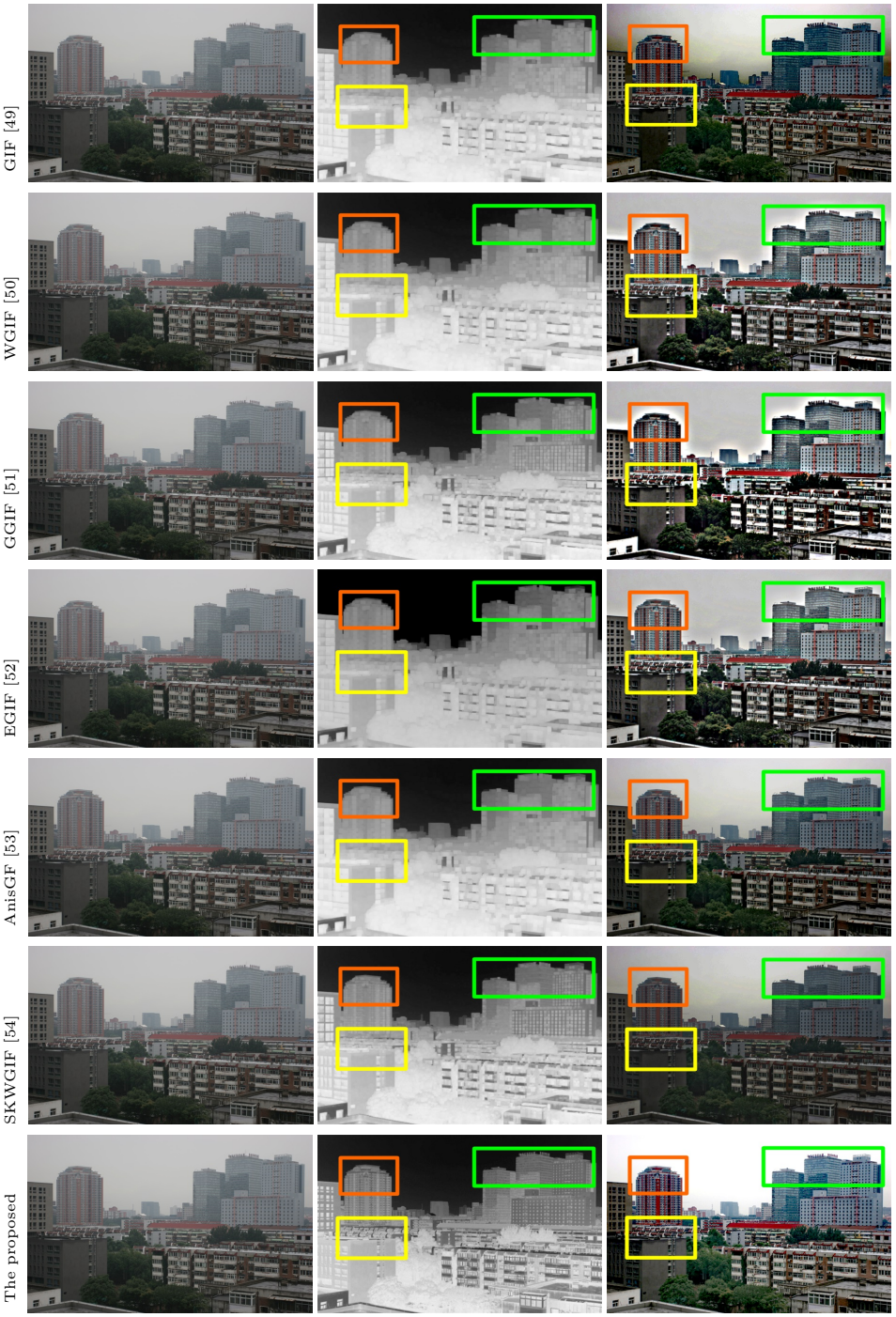

FIGURE 4.6: Refined transmission maps and corresponding dehaze outcomes different edge-preserving filters. For all figures, window size $\zeta_1 = 15$ and the regularization parameter $\varepsilon = 0.1^2$ is fixed. (a) Input hazy image, (b) Refined Transmission maps by different edge-preserving filters, (c) Dehazed output.

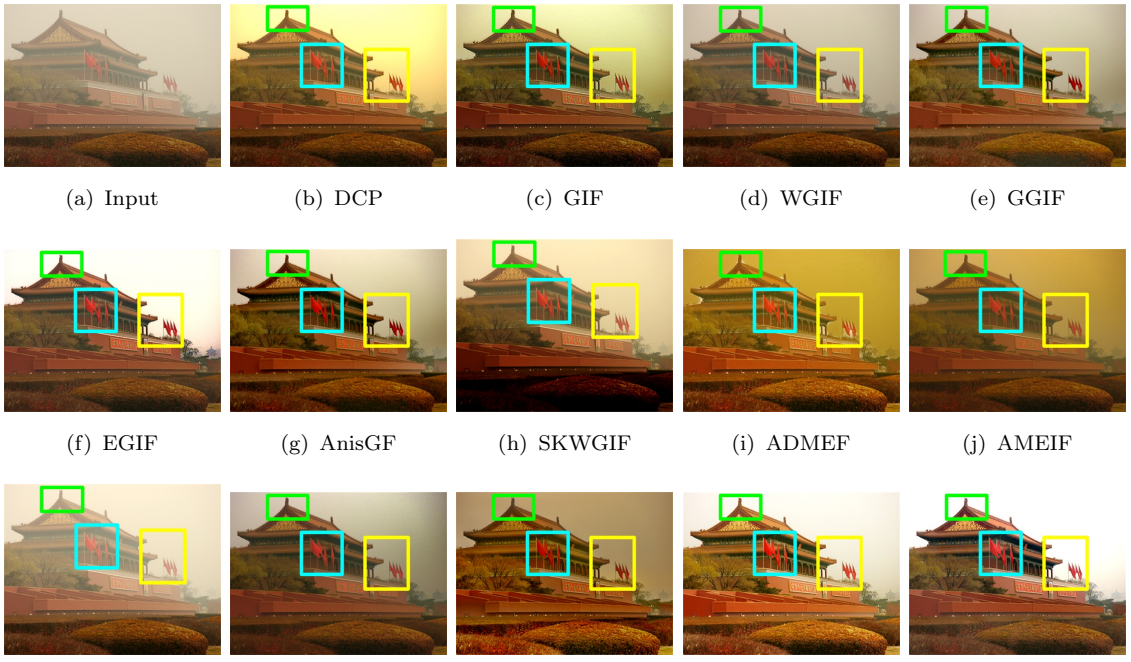

(a) Input (b) DCP (c) GIF (d) WGIF (e) GGIF

(f) EGIF (g) AnisGF (h) SKWGIF (i) ADMEF (j) AMEIF

(k) AOD-Net (l) RYF-Net (m) PMHLD (n) RefineDNet (o) Proposed

FIGURE 4.7: Dehazed outcomes of different haze removal methods.

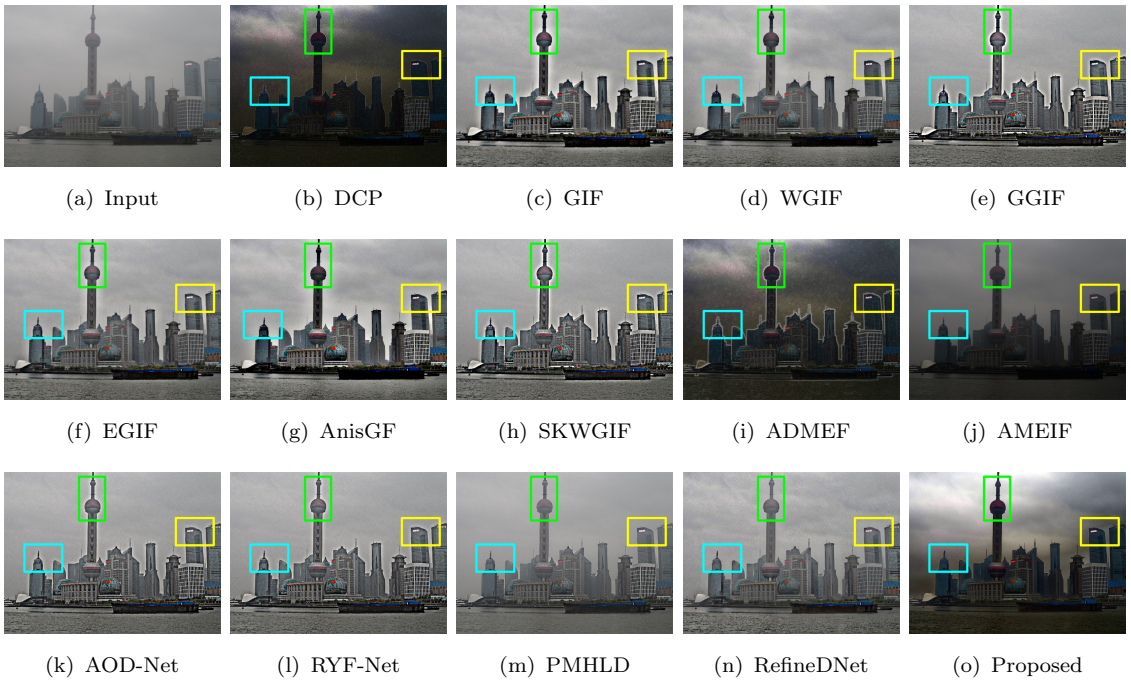

(a) Input (b) DCP (c) GIF (d) WGIF (e) GGIF

(f) EGIF (g) AnisGF (h) SKWGIF (i) ADMEF (j) AMEIF

(k) AOD-Net (l) RYF-Net (m) PMHLD (n) RefineDNet (o) Proposed

FIGURE 4.8: Dehazed outcomes of different haze removal methods.

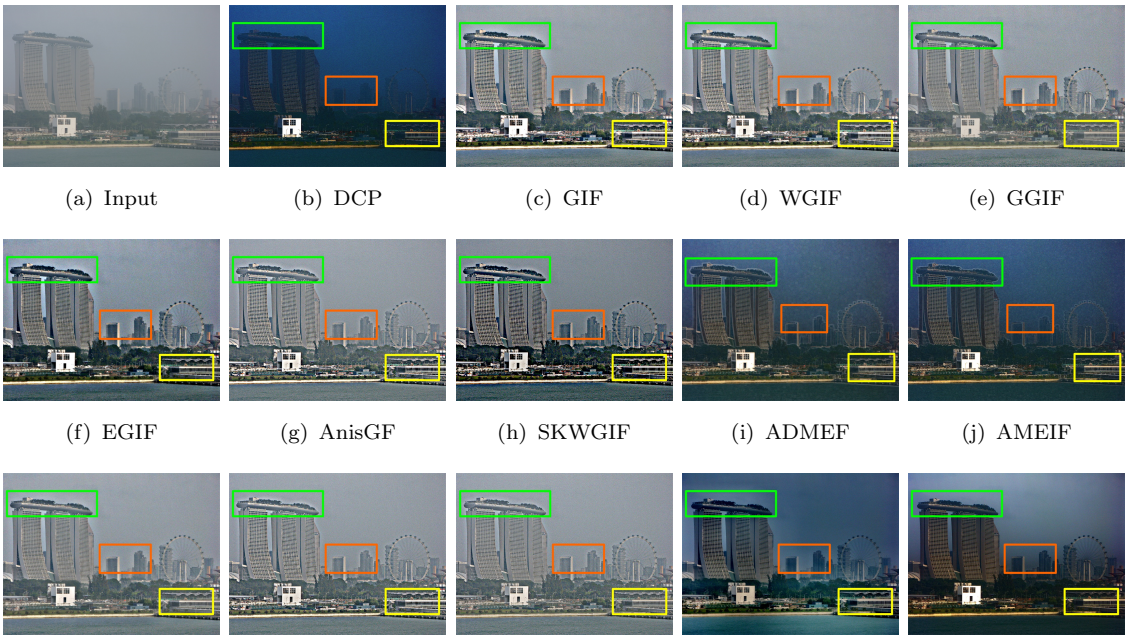

(a) Input (b) DCP (c) GIF (d) WGIF (e) GGIF

(f) EGIF (g) AnisGF (h) SKWGIF (i) ADMEF (j) AMEIF

(k) AOD-Net (l) RYF-Net (m) PMHLD (n) RefineDNet (o) Proposed

FIGURE 4.9: Dehazed outcomes of different haze removal methods.

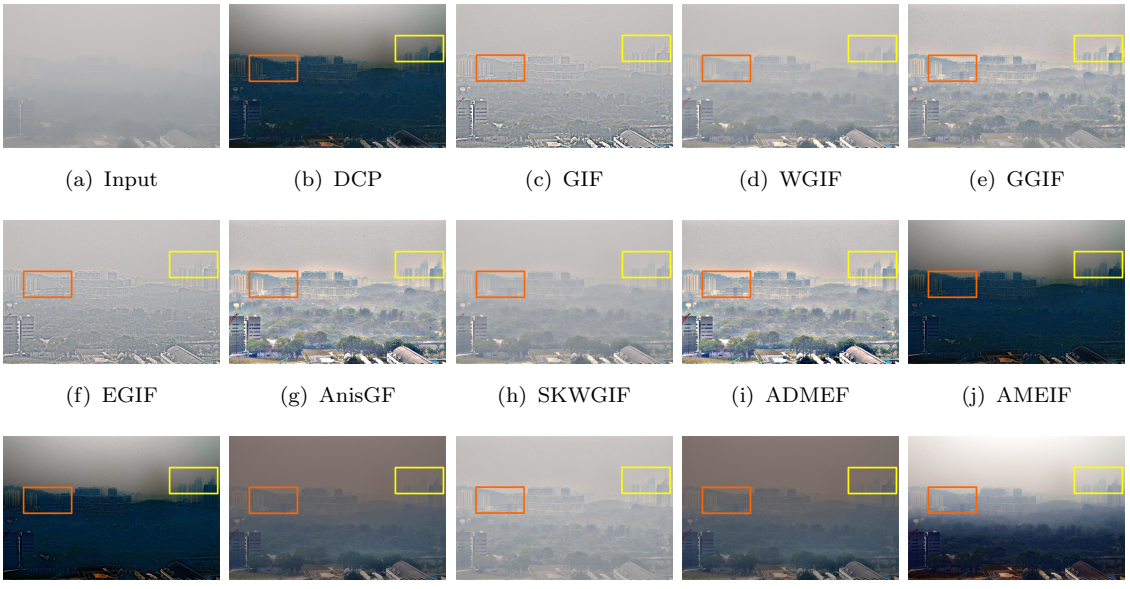

(a) Input (b) DCP (c) GIF (d) WGIF (e) GGIF

(f) EGIF (g) AnisGF (h) SKWGIF (i) ADMEF (j) AMEIF

(k) AOD-Net (l) RYF-Net (m) PMHLD (n) RefineDNet (o) Proposed

FIGURE 4.10: Dehazed outcomes of different haze removal methods.

global optimization image smoothing filter which removes halo artifacts and color distortions more strongly in both flat and sharp regions than the existing methods. Therefore, it also proves that the proposed method strongly remove halo artifacts and over-smoothing in both flat and sharp regions than [49], [50], [51], [52], [53], [54].

The proposed method has been tested on about 1,690 images from Fattal [16], D-HAZY [65], Middlebury [68], Haze-RD [69], Image-Net [77], NYU2 [66], FRIDA [67], O-HAZE [71] datasets and the dehaze outcomes are compared with 13 state-of-the-art haze removal methods out of which [15] is prior-based dehaze method, [49–54] are edge-preserving filter based haze removal methods, [33] and [35] are fusion based dehazing methods, and [38], [39], [41], and [42] are deep learning based haze removal methods. The visual comparison of the proposed method with the existing dehaze methods for 4 benchmark hazy images are illustrated in Figure 4.7-Figure 4.10. All the outcomes are calculated for window size ζ_1=15 and fixed regularization parameter $\varepsilon = 0.1^2$.

It is clear from these figures that the proposed method removes halo artifacts, over-smoothing strongly and preserve edge information more accurately in both flat and sharp regions than the existing [15], [49], [50], [51], [52], [53], [54], [33], [35], [38], [39], [41], and [42] methods. Over-smoothing increases with the increase in the regularization parameter ε. However, the proposed method does not suffer with such a problem. It is clear from Figure 4.7-Figure 4.10 that the proposed method provides more promising results than the existing methods. Since the proposed method is independent of the nature of image, it performs well on all the aforesaid datasets than the existing [15], [49], [50], [51], [52], [53], [54], [33], [35], [38], [39], [41], and [42] methods.

TABLE 4.1: Objective evaluation metric based assessment on tulip image

	GIF [49]	WGIF [50]	GGIF [51]	EGIF [52]	AnisGF [53]	SKWGIF [54]	Proposed
Input	36.87	36.87	36.87	36.87	36.87	36.87	36.87
$\varepsilon = 0.001^2$	**38.97**	**38.56**	37.69	37.48	37.82	37.04	37.15
$\varepsilon = 0.01^2$	40.25	40.07	43.26	43.51	39.11	**43.57**	**43.85**
$\varepsilon = 0.1^2$	34.33	32.18	43.21	43.09	32.47	**43.36**	**43.79**
$\varepsilon = 1^2$	28.86	27.64	41.39	40.75	27.44	**42.21**	**43.68**

TABLE 4.2: Performance comparison on Fattal dataset

Methods	e	$\overline{r}$	$\overline{\alpha}$	C_g	VCM	SSIM	PSNR	EKI	CIEDE 2000	FADE	CNI	UIQI
DCP [15]	5.13	1.31	0.18	0.051	66.13	0.7528	27.49	0.591	41.94	7.27	0.401	0.313
GIF [49]	6.34	1.75	0.14	0.168	68.05	0.7967	29.01	0.613	37.05	5.91	0.613	0.467
WGIF [50]	6.81	1.83	0.14	0.294	71.18	0.8118	30.62	0.647	35.12	5.15	0.673	0.549
GGIF [51]	10.35	1.89	0.12	0.385	74.31	0.8240	32.85	0.655	33.58	5.02	0.689	0.582
EGIF [52]	10.79	1.95	0.10	0.347	76.25	0.8251	32.82	0.692	32.41	4.88	0.697	0.597
AnisGF [53]	8.42	1.81	0.11	0.352	75.11	0.8295	31.05	0.657	33.02	4.54	0.708	0.609
SKWGIF [54]	9.41	1.99	0.11	0.386	76.68	0.8319	31.86	0.661	30.36	4.08	0.741	0.627
ADMEF [33]	10.10	2.06	0.12	0.449	76.89	0.8372	31.61	0.644	31.45	3.91	0.777	0.658
AMEIF [35]	11.27	2.36	0.11	0.482	76.93	0.8383	32.17	0.692	33.42	3.77	0.791	0.673
AOD-Net [38]	11.84	2.57	0.09	0.557	77.14	0.8521	32.49	0.695	33.87	3.21	0.794	0.698
RYF-Net [39]	12.38	3.40	0.10	0.598	77.56	0.8597	33.11	0.714	34.06	3.05	0.799	0.715
PMHLD [41]	13.52	4.25	**0.08**	0.662	78.49	0.8731	34.02	0.883	34.49	2.99	0.805	0.746
RefineDNet [42]	**13.89**	**4.87**	**0.08**	**0.690**	**78.88**	**0.8777**	**34.85**	**0.895**	**35.62**	**2.76**	**0.828**	**0.775**
Proposed	**16.05**	**5.39**	**0.06**	**0.753**	**80.25**	**0.8913**	**35.69**	**0.909**	**36.95**	**2.15**	**0.915**	**0.843**

4.3.2 Quantitative Analysis

We performed qualitative analysis of the proposed method to test and compare its performance. The results of this analysis are presented in this Section. We tested the quality of enhanced image using 4 different values of $\varepsilon = (0.001^2, 0.01^2, 0.1^2, 1^2)$ by an objective evaluation metric [83]. The enhancement scores of the proposed method and the existing [49], [50], [51], [52], [53], [54] methods for input tulip image [50] are furnished in Table 4.1. According to the objective evaluation metric [83],

TABLE 4.3: Performance comparison on D-Hazy dataset

Methods	e	$\overline{r}$	$\overline{\alpha}$	C_g	VCM	SSIM	PSNR	EKI	CIEDE 2000	FADE	CNI	UIQI
DCP [15]	4.70	1.05	0.21	0.119	49.26	0.6428	24.93	0.482	43.09	7.21	0.211	0.213
GIF [49]	4.91	1.17	0.19	0.197	51.93	0.6952	26.07	0.516	41.66	6.38	0.357	0.289
WGIF [50]	4.93	1.49	0.19	0.203	54.08	0.7115	26.85	0.537	41.28	6.02	0.396	0.326
GGIF [51]	5.27	1.51	0.17	0.244	56.11	0.7369	28.11	0.642	39.05	5.84	0.419	0.368
EGIF [52]	5.78	1.77	0.14	0.271	57.34	0.7530	28.82	0.679	37.24	5.11	0.477	0.391
AnisGF [53]	5.11	1.99	0.16	0.249	59.09	0.7445	29.06	0.618	34.51	4.92	0.501	0.427
SKWGIF [54]	5.19	2.23	0.15	0.282	61.57	0.7568	29.98	0.667	32.86	4.51	0.562	0.448
ADMEF [33]	5.39	2.89	0.16	0.308	62.95	0.7593	30.03	0.699	28.99	4.46	0.599	0.496
AMEIF [35]	7.01	3.16	0.13	0.366	64.44	0.7747	30.55	0.719	28.37	4.00	0.635	0.504
AOD-Net [38]	9.61	3.35	0.13	0.389	64.93	0.8165	31.88	0.782	27.58	3.91	0.709	0.565
RYF-Net [39]	10.38	3.80	0.11	0.524	67.01	0.8398	33.09	0.814	27.11	3.55	0.745	0.637
PMHLD [41]	12.57	4.18	0.09	0.695	67.92	0.8519	35.68	0.833	23.57	3.21	0.813	0.739
RefineDNet [42]	**12.85**	**4.75**	**0.08**	**0.705**	**68.55**	**0.8565**	**35.89**	**0.875**	**23.02**	**3.05**	**0.866**	**0.741**
Proposed	**13.69**	**6.48**	**0.05**	**0.738**	**69.92**	**0.8740**	**36.48**	**0.915**	**21.51**	**2.59**	**0.958**	**0.852**

TABLE 4.4: Performance comparison on Middlebury dataset

Methods	e	$\overline{r}$	$\overline{\alpha}$	C_g	VCM	SSIM	PSNR	EKI	CIEDE 2000	FADE	CNI	UIQI
DCP [15]	3.27	1.01	0.25	0.119	54.72	0.6648	24.82	0.495	42.25	7.69	0.255	0.292
GIF [49]	4.51	1.26	0.21	0.195	55.84	0.6815	26.37	0.518	41.58	6.95	0.425	0.357
WGIF [50]	4.90	1.49	0.21	0.198	56.85	0.6948	26.85	0.531	41.13	6.07	0.459	0.374
GGIF [51]	5.16	1.66	0.19	0.223	60.44	0.7212	28.42	0.573	40.62	5.75	0.493	0.427
EGIF [52]	5.22	1.85	0.18	0.279	62.88	0.7387	28.76	0.589	38.94	5.14	0.529	0.453
AnisGF [53]	6.10	1.99	0.19	0.296	64.65	0.7476	29.14	0.595	38.55	4.98	0.586	0.489
SKWGIF [54]	6.31	2.01	0.18	0.295	65.95	0.7495	29.82	0.618	38.11	4.65	0.628	0.501
ADMEF [33]	6.87	2.48	0.16	0.301	67.21	0.7520	29.99	0.637	36.49	4.16	0.667	0.524
AMEIF [35]	6.94	2.89	0.15	0.314	67.91	0.7573	30.84	0.661	35.25	3.99	0.704	0.551
AOD-Net [38]	7.08	3.45	0.14	0.389	70.35	0.7741	31.57	0.691	33.04	3.71	0.721	0.588
RYF-Net [39]	7.35	3.91	0.11	0.524	71.81	0.7805	33.09	0.714	31.47	3.25	0.746	0.617
PMHLD [41]	7.78	3.99	**0.10**	0.570	72.50	0.8026	33.85	0.735	31.01	3.04	0.773	0.636
RefineDNet [42]	**7.95**	**4.05**	**0.10**	**0.585**	**72.87**	**0.8135**	**34.00**	**0.778**	**29.52**	**2.89**	**0.791**	**0.670**
Proposed	**8.60**	**6.38**	**0.08**	**0.713**	**74.66**	**0.8464**	**35.45**	**0.925**	**25.09**	**2.15**	**0.808**	**0.775**

TABLE 4.5: Performance comparison on HazeRD dataset

Methods	e	$\overline{r}$	$\overline{\alpha}$	C_g	VCM	SSIM	PSNR	EKI	CIEDE 2000	FADE	CNI	UIQI
DCP [15]	3.95	1.62	0.28	0.105	52.59	0.6374	24.49	0.488	40.92	8.39	0.191	0.158
GIF [49]	4.20	1.99	0.25	0.139	55.31	0.6518	25.21	0.502	37.16	7.05	0.257	0.193
WGIF [50]	4.49	2.05	0.23	0.174	57.82	0.6792	25.89	0.561	36.29	6.89	0.284	0.266
GGIF [51]	4.71	2.84	0.21	0.198	62.09	0.7195	27.05	0.593	34.63	6.24	0.311	0.305
EGIF [52]	4.86	2.98	0.21	0.249	64.48	0.7417	27.96	0.625	31.97	5.98	0.369	0.337
AnisGF [53]	4.50	2.53	0.23	0.205	62.14	0.7053	26.34	0.608	31.22	5.25	0.394	0.378
SKWGIF [54]	4.62	2.58	0.22	0.217	62.83	0.7130	27.09	0.611	29.75	4.86	0.433	0.391
ADMEF [33]	5.09	2.96	0.19	0.284	66.81	0.7495	28.88	0.631	29.01	4.55	0.491	0.415
AMEIF [35]	5.85	2.98	0.18	0.401	67.11	0.7526	29.07	0.687	28.94	4.17	0.546	0.437
AOD-Net [38]	7.95	3.55	0.16	0.475	70.36	0.7618	31.69	0.705	28.43	3.64	0.544	0.445
RYF-Net [39]	8.24	3.83	0.15	0.538	70.89	0.7772	31.94	0.718	28.15	3.64	0.592	0.494
PMHLD [41]	9.38	4.12	**0.14**	0.590	71.21	0.7790	32.08	0.735	27.21	**2.76**	0.613	0.414
RefineDNet [42]	**9.80**	**4.25**	**0.14**	**0.625**	**71.84**	**0.7925**	**32.59**	**0.780**	**27.00**	2.15	**0.657**	**0.527**
Proposed	**11.35**	**4.40**	**0.12**	**0.745**	**72.08**	**0.8158**	**33.38**	**0.986**	**26.48**	2.98	**0.769**	**0.664**

TABLE 4.6: Performance comparison on Image-Net dataset

Methods	e	$\overline{r}$	$\overline{\alpha}$	C_g	VCM	SSIM	PSNR	EKI	CIEDE 2000	FADE	CNI	UIQI
DCP [15]	6.49	1.44	0.31	0.179	68.27	0.7338	27.05	0.574	38.41	7.59	0.211	0.131
GIF [49]	8.27	1.95	0.29	0.285	71.34	0.7521	29.11	0.613	36.85	6.81	0.236	0.159
WGIF [50]	8.60	2.30	0.28	0.297	71.86	0.7635	29.72	0.642	36.21	6.24	0.295	0.182
GGIF [51]	9.75	3.51	0.26	0.308	73.64	0.7784	31.47	0.686	35.79	5.93	0.351	0.197
EGIF [52]	9.87	3.97	0.26	0.346	74.45	0.7853	31.59	0.707	35.81	5.44	0.399	0.289
AnisGF [53]	9.95	3.58	0.27	0.311	74.26	0.7737	31.44	0.728	35.33	5.01	0.404	0.297
SKWGIF [54]	9.22	3.60	0.25	0.367	74.69	0.7952	31.95	0.753	31.04	4.75	0.482	0.348
ADMEF [33]	11.02	4.17	0.22	0.385	76.51	0.8211	32.01	0.764	30.51	4.26	0.513	0.386
AMEIF [35]	11.83	4.19	0.22	0.398	76.97	0.8399	32.66	0.787	30.27	4.11	0.562	0.390
AOD-Net [38]	13.48	4.20	0.21	0.401	78.64	0.8565	32.89	0.802	30.09	3.61	0.566	0.441
RYF-Net [39]	13.76	4.24	0.20	0.439	79.22	0.8589	32.95	0.818	30.04	3.05	0.581	0.495
PMHLD [41]	13.99	4.25	0.19	0.476	79.07	0.8620	33.21	0.839	30.00	3.00	0.592	0.502
RefineDNet [42]	**14.24**	**4.29**	**0.18**	**0.525**	**80.35**	**0.8677**	**33.75**	**0.890**	**29.64**	**2.95**	**0.625**	**0.578**
Proposed	**15.08**	**4.58**	**0.15**	**0.683**	**82.41**	**0.8818**	**34.16**	**0.937**	**27.35**	**2.35**	**0.686**	**0.609**

TABLE 4.7: Performance comparison on NYU2 dataset

Methods	e	$\overline{r}$	$\overline{\alpha}$	C_g	VCM	SSIM	PSNR	EKI	CIEDE 2000	FADE	CNI	UIQI
DCP [15]	6.13	1.57	0.26	0.195	70.63	0.7618	29.18	0.553	40.66	9.61	0.149	0.182
GIF [49]	9.05	2.30	0.24	0.267	73.19	0.7955	31.25	0.597	38.19	7.85	0.221	0.219
WGIF [50]	9.38	2.94	0.24	0.328	73.95	0.8314	31.59	0.625	37.58	7.26	0.295	0.276
GGIF [51]	10.27	3.87	0.23	0.379	75.55	0.8620	32.07	0.686	37.02	7.00	0.328	0.314
EGIF [52]	10.93	4.30	0.22	0.397	75.90	0.8757	32.82	0.724	37.02	6.39	0.385	0.356
AnisGF [53]	10.08	3.91	0.23	0.384	74.82	0.8713	32.44	0.695	38.31	5.96	0.392	0.385
SKWGIF [54]	10.54	4.06	0.22	0.372	75.40	0.8744	32.58	0.716	37.69	5.21	0.398	0.433
ADMEF [33]	12.73	4.22	0.20	0.399	76.28	0.8872	33.46	0.785	35.58	4.77	0.403	0.496
AMEIF [35]	12.65	4.68	0.18	0.402	78.11	0.8904	34.52	0.821	34.11	4.77	0.411	0.583
AOD-Net [38]	13.08	5.27	0.19	0.418	79.25	0.8908	34.80	0.869	34.87	4.48	0.420	0.636
RYF-Net [39]	13.69	5.39	0.17	0.479	81.51	0.8947	34.95	0.899	32.49	4.05	0.466	0.685
PMHLD [41]	14.25	5.39	**0.15**	0.515	81.81	0.8981	35.07	0.914	32.66	3.96	0.483	0.692
RefineDNet [42]	**14.91**	**6.02**	**0.15**	**0.568**	**82.08**	**0.9035**	**35.91**	**0.946**	**32.09**	**3.71**	**0.590**	**0.697**
Proposed	**16.77**	**6.95**	**0.13**	**0.675**	**83.65**	**0.9151**	**36.55**	**0.958**	**30.48**	**3.13**	**0.611**	**0.715**

TABLE 4.8: Performance comparison on FRIDA dataset

Methods	e	$\overline{r}$	$\overline{\alpha}$	C_g	VCM	SSIM	PSNR	EKI	CIEDE 2000	FADE	CNI	UIQI
DCP [15]	6.52	1.80	0.34	0.226	72.55	0.7814	29.84	0.581	41.38	8.69	0.375	0.115
GIF [49]	8.39	2.57	0.32	0.291	74.16	0.8062	31.79	0.616	40.02	7.25	0.460	0.183
WGIF [50]	8.68	2.97	0.32	0.339	74.59	0.8497	31.96	0.637	38.55	7.01	0.492	0.199
GGIF [51]	9.52	4.43	0.30	0.384	77.08	0.8991	32.81	0.675	38.13	6.57	0.518	0.205
EGIF [52]	11.82	5.26	0.28	0.425	77.96	0.9376	33.19	0.686	36.97	6.26	0.599	0.226
AnisGF [53]	9.85	3.72	0.26	0.351	75.59	0.8544	33.47	0.709	36.33	4.91	0.637	0.278
SKWGIF [54]	10.27	3.86	0.26	0.374	76.48	0.8695	33.98	0.718	35.69	4.38	0.675	0.319
ADMEF [33]	12.97	5.08	0.24	0.431	80.04	0.8662	34.04	0.734	33.08	4.11	0.741	0.394
AMEIF [35]	13.59	5.26	0.23	0.452	82.38	0.8910	34.25	0.739	33.01	3.85	0.779	0.422
AOD-Net [38]	13.94	5.59	0.21	0.469	82.55	0.8952	34.73	0.744	32.78	3.53	0.790	0.487
RYF-Net [39]	14.05	5.62	0.20	0.482	82.94	0.9015	34.80	0.768	32.11	3.20	0.801	0.495
PMHLD [41]	14.52	5.71	0.20	0.499	83.68	0.9138	34.91	0.779	30.52	3.00	0.835	0.517
RefineDNet [42]	**16.71**	**5.90**	**0.18**	**0.521**	**83.99**	**0.9185**	**35.11**	**0.790**	**29.61**	**2.68**	**0.884**	**0.538**
Proposed	**18.26**	**6.33**	**0.16**	**0.635**	**85.07**	**0.9285**	**36.24**	**0.824**	**27.52**	**2.25**	**0.925**	**0.745**

TABLE 4.9: Performance comparison on O-Haze dataset

Methods	e	$\overline{r}$	$\overline{\alpha}$	C_g	VCM	SSIM	PSNR	EKI	CIEDE 2000	FADE	CNI	UIQI
DCP [15]	8.02	1.89	0.51	0.291	73.08	0.7721	28.17	0.548	41.05	9.38	0.281	0.186
GIF [49]	11.46	2.79	0.48	0.352	74.77	0.7960	30.08	0.624	39.77	8.24	0.350	0.209
WGIF [50]	11.93	3.46	0.42	0.479	76.28	0.8011	31.79	0.658	39.14	8.07	0.418	0.268
GGIF [51]	13.21	3.75	0.40	0.498	77.59	0.8124	33.46	0.737	38.37	7.83	0.453	0.291
EGIF [52]	15.49	3.92	0.37	0.573	78.26	0.8169	35.88	0.783	38.11	7.51	0.488	0.327
AnisGF [53]	13.75	3.64	0.34	0.461	77.29	0.8205	34.65	0.694	37.68	6.80	0.510	0.385
SKWGIF [54]	14.47	3.89	0.31	0.479	77.95	0.8297	34.71	0.702	37.24	6.28	0.568	0.399
ADMEF [33]	15.83	5.34	0.29	0.494	78.34	0.8239	35.92	0.725	35.62	4.93	0.595	0.411
AMEIF [35]	17.06	5.86	0.28	0.511	79.31	0.8410	35.97	0.756	35.01	4.05	0.638	0.462
AOD-Net [38]	17.39	6.28	0.23	0.535	79.99	0.8465	36.60	0.769	32.55	3.66	0.694	0.481
RYF-Net [39]	17.95	6.91	0.20	0.549	80.34	0.8492	37.08	0.781	32.11	3.41	0.715	0.533
PMHLD [41]	18.02	6.99	0.19	0.568	80.86	0.8522	37.85	0.792	31.94	3.09	0.768	0.575
RefineDNet [42]	**18.64**	**7.22**	**0.17**	**0.573**	**82.54**	**0.8579**	**37.91**	**0.805**	**29.85**	**2.99**	**0.793**	**0.608**
Proposed	**19.33**	**8.53**	**0.15**	**0.659**	**84.79**	**0.8708**	**38.24**	**0.886**	**28.05**	**2.15**	**0.885**	**0.769**

TABLE 4.10: Average execution time (in seconds) based assessment

Methods	185×231	384×512	512×768	600×450	1600×1200	2592×1944	2144×1424	2300×1600
DCP [15]	2.25	6.38	9.79	11.95	19.08	26.85	22.97	24.05
GIF [49]	1.13	4.74	7.66	9.83	15.94	22.05	20.69	23.88
WGIF [50]	1.04	4.26	7.59	9.77	15.06	21.79	20.42	23.64
GGIF [51]	0.95	4.21	7.47	8.59	13.98	20.61	19.55	22.71
EGIF [52]	0.95	4.19	7.43	8.51	13.90	20.45	19.31	22.53
AnisGF [53]	1.03	4.25	7.55	9.68	14.05	22.52	20.15	23.38
SKWGIF [54]	1.06	4.20	7.51	9.56	14.93	22.81	20.64	23.67
ADMEF [33]	0.90	4.16	6.36	8.34	14.84	21.49	19.57	22.84
AMEIF [35]	0.91	4.10	6.29	8.21	14.77	21.15	19.02	21.45
AOD-Net [38]	0.88	4.03	6.23	8.69	13.59	19.68	18.77	21.08
RYF-Net [39]	0.86	3.97	6.19	8.01	13.35	20.96	18.06	20.29
PMHLD [41]	**0.81**	3.93	5.12	7.99	12.91	19.24	18.48	**19.26**
RefineDNet [42]	0.89	**3.91**	**5.07**	**6.71**	**12.04**	**18.68**	**17.30**	20.04
Proposed	**0.77**	**2.88**	**3.91**	**6.94**	**10.28**	**15.48**	**12.97**	**15.89**

the quality of the enhanced image is represented by higher scores. It is clear from Table 4.1 that initially scores of enhanced image has increased and later on it decreased with increase in ε value. Over-smoothness near the sharp regions is the main reason for the lower score in the enhanced images. The red and blue bold values in Table 4.1 indicate the best and second-best score, respectively. It is clear from Table 4.1 that the proposed method has highest score than the existing [49], [50], [51], [52], [53], [54] methods for all ε values except ε=0.001^2. Further, the scores of [49] and [50] fall rapidly and they even fall below the input score. But, the score of images enhanced with [51], [52], [53], [54] and the proposed method do not fall below the input score. It is also evident from Table 4.1 that the proposed method has better score for a given ε values and the scores are superior than the existing [49], [50], [51], [52], [53], and [54] methods.

The performance metrics e [79], $\overline{r}$ [79], $\overline{\alpha}$ [79], contrast gain C_g [85], visual contrast measurement (VCM) [80], structural similarity index (SSIM) [86], peak signal to noise ratio (PSNR) [87], edge keeping index (EKI) [88], color difference metric CIEDE2000 [89], fog aware density evaluator (FADE) [81], color natural index (CNI) [82], and universal image quality index (UIQI) [90] are used to assess the effectiveness of the proposed method more judiciously. The average performance metrics scores of the proposed method with the existing [15], [49], [50], [51], [52], [53], [54], [33], [35], [38], [39], [41], [42] methods are evaluated for hazy, non-hazy, synthetic images from 8 datasets viz. Fattal [16], D-HAZY [65], Middlebury [68], Haze-RD [69], Image-Net [77], NYU2 [66], FRIDA [67], O-HAZE [71] and their results are furnished in Table 4.2 to Table 4.9, respectively.

The red and blue bold values in Table 4.2 to Table 4.9 indicate best and second-best performance, respectively. These results clearly state that the proposed method has

the highest e and $\overline{r}$ values and the least $\overline{\alpha}$ values than the existing methods, as expected. However, deep learning based [41] and [42] methods have also better e, $\overline{r}$, and $\overline{\alpha}$ values than the rest of the existing methods. The best score of e, $\overline{r}$ and $\overline{\alpha}$ for Fattal [16], D-HAZY [65], Middlebury [68], Haze-RD [69], Image-Net [77], NYU2 [66], FRIDA [67], and O-HAZE [71] datasets are (16.05, 13.69, 8.60, 11.35, 15.08, 16.77, 18.26, 19.23), (5.39, 6.48, 6.38, 4.40, 4.58, 6.95, 6.33, 8.53) and (0.06, 0.05, 0.08, 0.12, 0.15, 0.13, 0.16, 0.15), respectively.

Next, the contrast gain C_g and visual contrast measurement (VCM) metrics are calculated. The contrast gain C_g [85] measures the contrast of dehazed image and larger value of C_{g} indicates the higher contrast of dehaze image. The visual contrast measurement (VCM) [80] metric evaluates the visual quality of the restored image and larger the VCM value indicates the better visibility of the recovered image. It is clear from Table 4.2 to Table 4.9 that the proposed method and RefineDNet [42] have highest and second-highest C_g and VCM values than the rest of the existing methods. The best C_g and VCM scores for Fattal [16], D-HAZY [65], Middlebury [68], Haze-RD [69], Image-Net [77], NYU2 [66], FRIDA [67], and O-HAZE [71] datasets are (0.753, 0.738, 0.713, 0.745, 0.683, 0.675, 0.635, 0.659) and (80.25, 69.92, 74.66, 72.08, 82.41, 83.65, 85.07, 84.79), respectively.

It is clear from Table 4.2 to Table 4.9 that the proposed method has the highest structural similarity index (SSIM) [86], peak signal to noise ratio (PSNR) [87] and edge keeping index (EKI) [88] values than the rest of the existing methods. The best SSIM, PSNR and EKI values Fattal, D-HAZY, Middlebury, Haze-RD, Image-Net, NYU2, FRIDA, and O-HAZE datasets are (0.8913, 0.8740, 0.8464, 0.8158, 0.8818, 0.9151, 0.9285, 0.8708), (35.69, 36.48, 35.45, 33.38, 34.16, 36.55, 36.24, 38.24), and (0.909, 0.915, 0.925, 0.986, 0.937, 0.958, 0.824, 0.886), respectively.

Further, the proposed method has the least color difference metric CIEDE2000 [89] and fog aware density evaluator (FADE) [81] scores than the existing methods. The best CIEDE2000 and FADE values for Fattal, D-HAZY, Middlebury, Haze-RD, Image-Net, NYU2, FRIDA, and O-HAZE datasets are (36.95, 21.51, 25.09, 26.48, 27.35, 30.48, 27.52, 28.05), and (2.15, 2.59, 2.15, 2.15, 2.35, 3.13, 2.25, 2.15), respectively.

Next, it is clear from Table 4.2 to Table 4.9 that the proposed method has the highest color natural index (CNI) [82] and universal image quality index (UIQI) [90] than the existing methods. The best CNI and UIQI scores Fattal, D-HAZY, Middlebury, Haze-RD, Image-Net, NYU2, FRIDA, and O-HAZE datasets are (0.915, 0.958, 0.808, 0.769, 0.686, 0.611, 0.925, 0.885), and (0.843, 0.852, 0.775, 0.664, 0.609, 0.715, 0.745, 0.769), respectively.

In addition to these metrics, we calculated the average execution time of the proposed method with the existing [15], [49], [50], [51], [52], [53], [54], [33], [35], [38], [39], [41], [42] methods for [16], [65], [68], [69], [77], [66], [67], [71] datasets. For this purpose, we selected 10 images from each dataset with resolutions of 185 $\times$ 231, 384 $\times$ 512, 512 $\times$ 768, 600 $\times$ 450, 1600 $\times$ 1200, 2592 $\times$ 1944, 2144 $\times$ 1424, and 2300 $\times$ 1600 and their results are furnished in Table 4.10. The bold values in red and blue indicate the best and second-best performance, respectively. The proposed method and deep learning based [41], [42] methods have better execution time than the rest of existing methods. However, the proposed method has fast average execution time for all resolutions of image except 600 $\times$ 450 resolution of image. It is evident from these results that the proposed method is the fastest than the existing methods for a given resolution of the image.

The statistical assessment of the proposed method with the existing [15], [49], [50], [51], [52], [53], [54], [33], [35], [38], [39], [41], [42] methods are evaluated using box plot [92] for 12 performance metrics; e, $\overline{r}$, $\overline{\alpha}$, C_g, VCM, SSIM, PSNR, EKI, CIEDE2000, FADE, CNI, UIQI and their outcomes are shown in Figure 4.11 to Figure 4.12. The horizontal line within the box plot represents the median value. It is observed from the box plots that the median value of the proposed method is the highest in e, $\overline{r}$, C_g, VCM, SSIM, PSNR, EKI, CNI, UIQI and the least in $\overline{\alpha}$, CIEDE2000, FADE performance metrics than the existing methods, as expected. Thus, it proves that the proposed method is better than existing [15], [49], [50], [51], [52], [53], [54], [33], [35], [38], [39], [41], [42] methods.

4.4 Limitations

Image dehazing is a challenging task due to the complex physical and optically properties of haze which can produce inconsistencies in the image. Additionally, the inhomogeneous transmission of light into and through the atmosphere can be affected by variable weather conditions making the haze removal problem more difficult. In this chapter, we have proposed a robust edge-weighting gradient guided filter for single image dehazing. It removes halos and over-smoothing strongly and preserves edge information efficiently. However, it fail in case of dense hazy images.

4.5 Concluding Remarks

In this work, a new robust scale-aware weighting-based effective edge-preserving gradient domain guided image filter is proposed for single image dehazing. It is

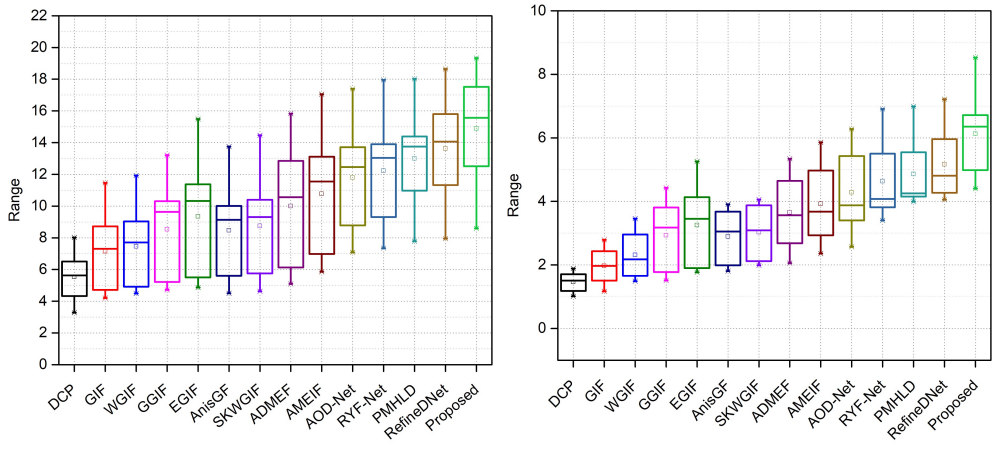

(a) e [79] (b) $\overline{r}$ [79]

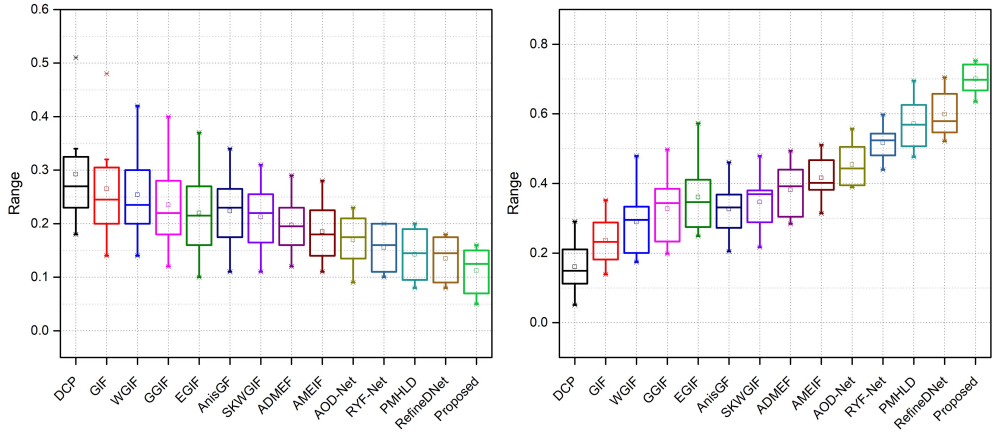

(c) $\overline{\alpha}$ [79] (d) C_g [85]

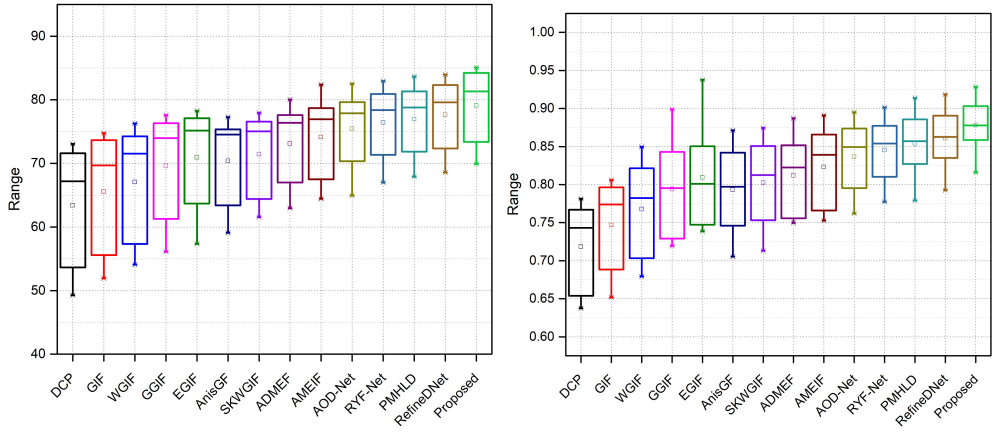

(e) VCM [80] (f) SSIM [86]

FIGURE 4.11: Statistical illustration of different haze removal methods and the proposed method using box plot.

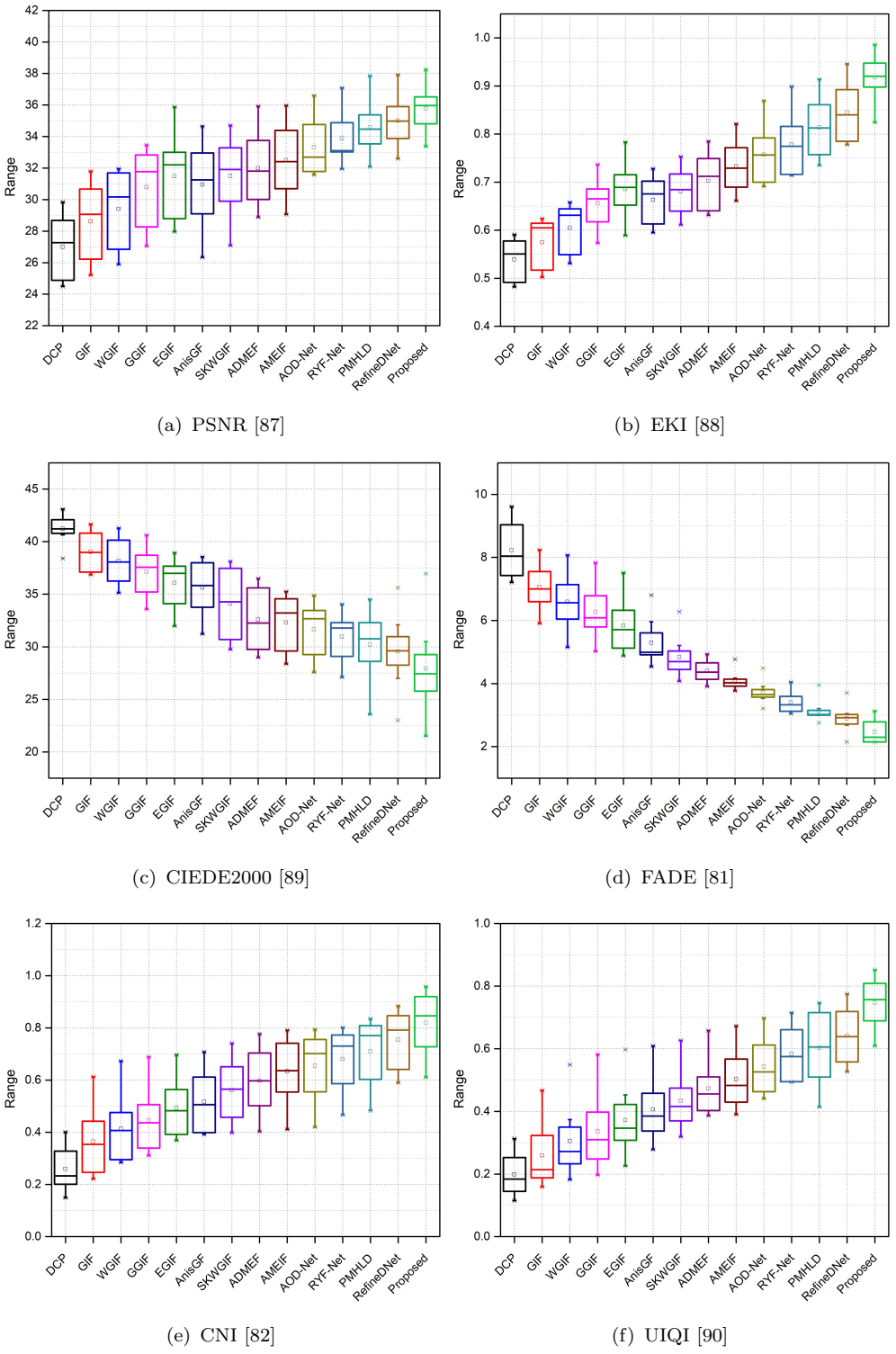

(a) PSNR [87]

(b) EKI [88]

(c) CIEDE2000 [89]

(d) FADE [81]

(e) CNI [82]

(f) UIQI [90]

FIGURE 4.12: Statistical illustration of different haze removal methods and the proposed method using box plot.

an effective haze removal approach which removes halo artifacts, over-smoothing strongly and preserves edge information precisely in both flat and sharp regions. The performance of the proposed method is tested on about 1,690 images from Fattal [16], D-HAZY [65], Middlebury [68], Haze-RD [69], Image-Net [77], NYU2 [66], FRIDA [67], O-HAZE [71] datasets and the dehazed outcomes are compared with 13 state-of-the-art [15], [49], [50], [51], [52], [53], [54], [33], [35], [38], [39], [41], [42] haze removal methods. It is evident from Figure 4.3 to Figure 4.10 that dehazed outcome of the proposed method is superior than the existing methods.

Finally, qualitative analysis proves that the proposed method is independent of the nature of image and it performs equally well for all datasets as compared to the existing image dehazing methods. The quantity analysis shown in Table 4.1 to Table 4.9, also proves that the proposed method is better than the existing methods. Results of average execution time, listed in Table 4.10, also demonstrate that the proposed method requires less processing time as compared to the existing methods. The box plot based statistical assessment of the proposed method is shown in Figure 4.11 and Figure 4.12 for different performance metrics namely e, $\overline{r}$, $\overline{\alpha}$, C_g, VCM, SSIM, PSNR, EKI, CIEDE2000, FADE, CNI, and UIQI prove that performance of the proposed method is better than the existing methods. From all these facts, it is clear that the proposed method removes halo artifacts, over-smoothing, color distortion strongly and preserves edge information precisely in both flat as well as sharp regions.